ELSEVIER

Contents lists available at ScienceDirect

Materialia

journal homepage: www.elsevier.com/locate/mtla



Full Length Article

A general indicator for the tolerance to impurities of metals and alloys

Ethen Thomas Lund ^a, Salena Huang ^a, Sebastian A. Kube ^{a,b}, Guannan Liu ^a, Nathan Johnson ^c, Wade Colley ^a, Apurva Mehta ^c, Barbara K. Reck ^d, Sungwoo Sohn ^{a,*}, Jan Schroers ^{a,*}

- ^a Department of Mechanical Engineering and Materials Science, Yale University, New Haven CT 06511, USA
- ^b Materials Department, University of California, Santa Barbara CA 93106, USA
- ^c Stanford Synchrotron Radiation Lightsource, SLAC National Accelerator Laboratory, Menlo Park CA 94025, USA
- ^d School of the Environment, Yale University, New Haven CT 06511, USA

ARTICLE INFO

Keywords: Combinatorial materials science Metals Recycling Metallic glasses Impurity tolerance

ABSTRACT

The tolerances of alloys to impurities can vary significantly across impurity-alloy combinations and are largely unknown beyond the most common alloys and impurities. Further, a more general framework to quantify, compare, and practically utilize the tolerance of elements and alloys to impurities is missing. Here, we propose such a framework based on the parameter $C_{\rm IM}$, the maximum content of an impurity that can be added to a pure element before it no longer crystallizes and instead vitrifies, as measured under sputtering conditions. Using high throughput combinatorial methods, $C_{\rm IM}$ can be readily determined for practically important impurity-element combinations. We argue that $C_{\rm IM}$ generally indicates impurity tolerance because it ubiquitously measures solid solution stability and provide arguments on how conclusions may be drawn from impurity-element to impurity-alloy tolerance. This practical metric for evaluating impurity tolerances for alloys may help metallurgy by enabling greater recycled feedstock compatibility during manufacturing and, in the future, the design of more impurity tolerant alloys.

1. Introduction

Managing impurity content in the extraction, recycling, and processing of alloys is motivated by the metallurgical industry's vast environmental impact, accounting for ~8 % of global energy consumption and ~30 % of industrial CO₂ equivalent emissions annually [1]. Most of this impact originates from the primary production and purification of elemental metals from ores, and thus, could be significantly reduced by the effective recycling of metals and alloys and, in the future, the development of novel impurity tolerant alloys. However, recycling inevitably introduces unwanted impurities to alloys via the existing alloying elements of the recycling stream and contaminants introduced during the processing of the materials. This poses a problem for today's alloys, which are compositionally highly engineered, often composed of five or more elements, with quantities often specified down to fractions of an atomic percent. This requires tight controls on compositional deviations and impurities arising from the metal extraction processes [2, 3], recycling streams [4], and alloy processing [5,6], with standardized impurity thresholds often defined down to 0.1 atomic% in physical and chemical metallurgy processes. However, these thresholds are ill-defined for the many potential impurities introduced by recycling.

Specific effects of impurities on alloy properties have been determined in detail for some of the most prominent alloys based on iron [7–10] and aluminum [11–13]. For example, the effect on iron and some steel alloys of some small quantity of elements originating from primary extraction, recycling, and processing including Cu, Cr, Nb, Mn, V, Mo, P, and S have been studied thoroughly [7,14,15]. Such studies include evaluation of mechanical properties [15–17], microstructure [18], corrosion properties [19], machinability [20], magnetic properties [21], creep properties [17], fracture toughness [16,22], and fatigue [17]. However, beyond this very specific knowledge, in general, it is mostly unknown what effect impurities have on an alloys' properties. Significant time, effort, and resources are required to manually characterize impurity effects, and existing computational models have been unable to fully capture the behavior of highly contaminated compositions, leaving a gap in understanding.

This unpredictability can often lead to manufacturer hesitancy in accepted recycled scrap feedstock, which is generally of slightly lower purity than primary feedstock. These different and, at times, dramatic effects on an alloy's measurable properties due to impurities [23–31] is

E-mail addresses: sungwoo.sohn@yale.edu (S. Sohn), jan.schroers@yale.edu (J. Schroers).

https://doi.org/10.1016/j.mtla.2024.102037

^{*} Corresponding authors.

referred to as impurity tolerance. Impurity tolerance can be generally described by how much of a given impurity can be added to an alloy without a noticeable change in its microstructure and properties. Alloys' properties, including strength, ductility, and creep, are affected by the impurity through the microstructure, where impurities can influence the nucleation and growth process, which can lead to the formation of new phases [32], changes in the grain size and texture [29,33], altered chemistry of existing phases [26], and affects grain boundary chemistry [34].

Reducing impurity content in extraction, recycling, and processing is an active area of research, but every available method necessarily increases costs, energy use, or the generation of often harmful by-products [35,36]. To reduce the environmental impact of metallurgy, a focus has emerged on developing alloys that are more tolerant of compositional impurities [36–39]. Such alloys could tolerate higher scrap shares as input material, in turn reducing the energy demand in alloy production [40,41], and the demand for primary raw materials, an advantage given that many alloying elements are considered critical [42–44] and may not easily be available in the future. This approach would enable greater adoption of the existing Principles of Green Engineering framework in industrial metallurgy, enabling engineers to conserve the complexity of alloys rather than separate them into component streams and design alloys for commercial afterlives rather than single use. [45]

This study presents an approach to facilitate these goals of improved recyclability and alloy design: a basic, high-level tool to estimate effects of impurities on alloys. This is important for effective, flexible, and sustainable metallurgy and hence, could have a sizeable impact writ large on the sustainability of metallurgical practices. However, because this indicator is based on the general structural effects of impurities, alloy-specific effects, including precise changes in properties will not be fully captured. Instead, an analysis is presented on drawing general conclusions on impurity-alloy effects using the here presented structural impurity tolerance indicator.

1.1. Quantifying impurity tolerance through C_{IM}

The effects of impurities on alloy properties are often highly complex and system specific. However, there are also general features of an impurity that indicate its general impact. Identifying quantitative measurements for such general behavior is the focus of this work. Structurally, impurities can impact an alloy by destabilizing the base metal's solid solution. If the effect of the impurity is minor, it does little to destabilize and instead dissolves into the solid solution. If the effect is stronger, the impurity can impact the crystal lattice, leading to solid solution strengthening, or rejection from the phase altogether, leading to new precipitates or collection at the grain boundary. Such effects may be described by atomic dispersity, a unified dimension representing the difference between elements in characteristics or properties which govern a behavior of interest, in this case being phase selection [46]. We argue that the effect of an impurity on a base metal or alloy increases with the quantity of the impurity and its dispersity from the metal or alloy. Hence, the effect of an impurity on a base metal could be quantified by (for a given impurity-base pair, i.e., constant dispersity) the content of impurity that can be added to a base before a measurable change occurs. A general measure of this effect is the change in the solidification path from crystalline to amorphous, when the impurity destabilizes the base metal sufficiently to the extent that it can no longer crystallize. At this well-defined and generally occurring transition, the content of impurity at which the transition occurs, C_{IM} , is used as the metric to indicate impurity tolerance.

For example, if the atomic dispersity between impurity and base metal is low, one can expect that the base can tolerate a large fraction of impurity without significantly affecting its solidification. In that case, a large $C_{\rm IM}$ would be observed. On the other hand, if the atomic dispersity between impurity and base is high, small amounts of impurity will have a strong effect on the solidification path. Here, $C_{\rm IM}$ will be small.

Thereby, $C_{\rm IM}$ indicates the tolerance of a base element or alloy to the impurity. It is important to mention that such tolerance is not quantitatively predictive of specific property changes. Instead, $C_{\rm IM}$ only suggests the tendency or likelihood of an effect. Hence, $C_{\rm IM}$ represents a high-level indicator, rather than a substitute to the existing and highly detailed case by case impurity-effect-on-alloy characterization methods. The key advantage of proposed $C_{\rm IM}$ method is that it can be readily determined, hence providing a tool that can estimate and pre-scan the impact of an impurity on an alloy prior to fabricating it and do so for a vast range of multicomponent alloys. Further, when using $C_{\rm IM}$ to discuss impurity tolerance, it is important to acknowledge that only the relative values of the $C_{\rm IM}$ have meaning and can be used to estimate impurity tolerance. The absolute values of $C_{\rm IM}$ are dependent on the cooling rate used to determine $C_{\rm IM}$ and are therefore arbitrary without specification of the underlying cooling rate.

2. Experimental

To observe a crystalline-amorphous transition and thereby measure $C_{\rm IM}$, an appropriate cooling rate for sample fabrication must be chosen. If a cooling rate that is too slow is chosen, all impurity-base element compositions will crystallize, and $C_{\rm IM}=100$ % will be measured for all binary combinations. If the cooling rate is too fast, all alloys will vitrify into a glass, and $C_{\rm IM}=0$ % will be measured. In both scenarios, there will be no measured distinction between alloys, and therefore no measurement of impurity tolerance. To most sensitively measure $C_{\rm IM}$, the highest differentiation between vitrification and crystallization is preferred. The corresponding cooling rate for such a differentiation has been previously estimated to be in the range 10^8-10^{10} K/s [47], which can be realized through sputtering. Therefore, we propose the use of thin film sputtering to reveal the differences in impurity tolerance through $C_{\rm IM}$, as it is a practical fabrication technique with a cooling rate of $\sim 10^8$ K/s.

Further, it is important that an indicator for impurity tolerance is practical and can be determined on a reasonable time scale for most element-impurity combinations. As a broad approximation, \sim 45 elements should be considered as they constitute the vast majority of practical alloying elements and their common impurities [48,49]. Their binary combinations, element A in element B and conversely B in A, account for 1980 binary combinations in 990 binary systems. Assuming a necessary compositional resolution of \sim 1 % to distinguish between alloys results in \sim 10⁵ alloys. This quantity of alloys is by many orders of magnitude too large to be fabricated and characterized with conventional techniques. However, it can be considered on a reasonable time scale by combinatorial sputtering (Fig. 1).

Binary alloy libraries are sputtered using magnetron co-sputtering (Fig. 1a). With a two target setup, 66 binary alloys of composition from $\sim\!A_{95}B_5$ to $\sim\!A_5B_{95}$ are fabricated [50]. To correlate the position in the library with the chemical composition, EDX is carried out (Fig. 1b). XRD is used to determine if the alloys in the library are amorphous or crystalline (Fig. 1c). For a consistent evaluation of C_{IM} , we choose a volume fraction of $\sim\!50$ % amorphous as indicated by the broadening of the main diffraction peak to double of the width of the crystalline peak (Supplementary Methods 1).

To obtain a first representative fraction of all 1980 element-impurity combinations, the fabrication of 110 element-(metal)impurity combinations (57 binary systems) is presented here. Within each binary system, we realized 66 alloys, which amount to ~3800 element-impurity alloys for which we measured composition (EDX) and structure (XRD). For four Al-based impurity combinations, bulk samples are fabricated, and their microstructures are characterized (Supplementary Figure 1). Those microstructures are used as a first assessment of the impurity tolerance indicator by comparing the effects of absolute compositions and solidification conditions on bulk alloys (Supplementary Figure 2).

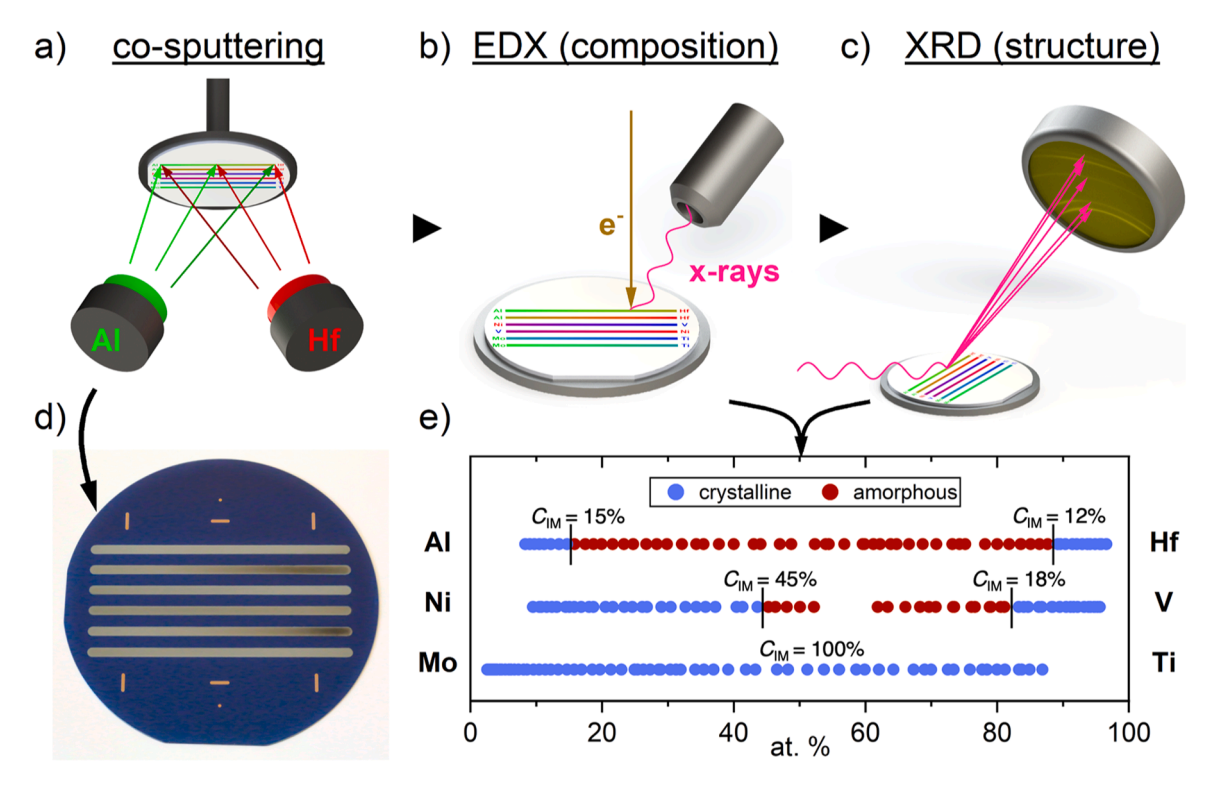


Fig. 1. Combinatorial synthesis and high-throughput characterization of element-impurity combinations. a) Combinatorial synthesis is used to fabricate binary combinations of elements, realizing 66 unique compositions per binary system. b) EDX is used to determine the chemical composition of the alloys, and c) XRD is used to determine the atomic structure and distinguish between amorphous and crystalline compositions. Example 4" wafer (d) and evaluation summaries (e), showing crystalline-amorphous transitions in Al-Hf, with $C_{\rm IM}^{\rm Ali}$ in $^{\rm Hf}$ = 12% and $C_{\rm IM}^{\rm Hf}$ in $^{\rm Al}$ = 15%, and Ni-V, with $C_{\rm IM}^{\rm Ni}$ in $^{\rm V}$ = 18% and $C_{\rm IM}^{\rm V}$ in $^{\rm Ni}$ = 45%. For the Mo-Ti alloy, all combinations crystallize during sputtering, hence $C_{\rm IM}^{\rm Cu}$ in $^{\rm Ni}$ in $^{\rm Cu}$ = 100%. The density and distribution of the data points are determined by the angles and intensity of the combinatorial guns shown in (a), leading to compositional resolution of $^{\rm Cu}$ at.% for areas of interest. (color in print & online).

2.1. Methods

2.1.1. Combinatorial co-sputtering fabrication

The binary alloy libraries were created by confocal DC Magnetron co-sputtering (AJA International ATC2200), with the sputtering guns and substrate arranged as depicted in Fig. 1a. Sputtering targets of purity 99.95 % or greater were used (AJA International and Kurt J. Lesker Company). Wafers of 4" diameter were used as substrates (UniversityWafer Inc.). Sapphire wafers were used for binaries including Si, and silicon wafers with 1 µm of thermal oxide were used for all other binaries. Substrates were covered with steel masks of 0.01" thickness to limit the deposition to rows with height of 3 mm and length of 83 mm. Each AB binary system was deposited as a compositional gradient over two separate rows, with the first spanning compositions ~A₅B₉₅ to $A_{50}B_{50}$ and the second spanning $\sim A_{50}B_{50}$ to $A_{95}B_5$. These compositions were tailored by adjusting the deposition rates of the sources using the applied power. Prior to sputtering, the chamber was evacuated to a pressure level of 5.0×10^{-7} Torr. The films were then sputtered in flowing ultra-high purity argon gas at a pressure of 5.8×10^{-3} Torr.

High-throughput characterization: Characterization of the compositional gradient rows was performed using EDX (Helios G4 Focused Ion Beam – Scanning Electron Microscopy with UltraDry EDX detector, 25 kV accelerating voltage) and XRD (Stanford Synchrotron Radiation Lightsource (SSRL) at SLAC National Accelerator Laboratory, beamline 1–5, 12.7 keV photon energy) with automated routines that controlled xy-position, taking measurements every 2.5 mm along the length of each row.

2.1.2. Microstructure analysis

Bulk samples were fabricated from pure elements (Alfa Aesar, Al: 99.99 %, Au: 99.99 %, Fe: 99.99 %, Ni: 99.95 %, V: 99.7 %) via arc

melting furnace (Edmund Bühler GmbH, model: AM200) in a purified-Ar gas, Ti gettered atmosphere on a water-cooled Cu plate. Each alloy was cut into 2 pieces, of which one was cold rolled to 50 % strain then annealed at 70 % of the melting temperature for 16 h and one was arcmelted and suction cast into 1 mm and 4 mm cylinders in a water-cooled Cu mold (Edmund Bühler GmbH, model: MAM-1). Samples were then mounted in a two-part epoxy, polished to a mirror finish using sandpaper and then suspended colloidal solutions down to 3 μm grit, and imaged at x2000 under SEM-Backscattered Electron imaging (Hitachi SU7000). Microstructures are characterized via the mean lineal intercept length of the α phase (\bar{l}_{α}) using ImageJ using 5 fields of measurement per sample, as detailed in ASTM E112. Error bars in Fig. 5 are the upper and lower 95 % confidence intervals.

3. Results

Using this approach, 110 element-impurity have been characterized. This fraction of $\sim\!\!6$ % of all practical element-impurity combinations constitutes a representative fraction of the element-(metal) impurity combinations and allows us to introduce and preliminarily access $C_{\rm IM}$ as a general indicator for impurity. An example system, Ni-V, is shown in Fig. 2. For compositions Ni $_{\rm X}$ V100- $_{\rm X}$ where x>81, the as-sputtered alloys form an FCC structure, as indicated by the XRD diffractogram (Fig 2.c.i). For 45 < x < 81, the as-sputtered alloys in this alloy system form an amorphous phase (Fig. 2.c.ii), and for alloys with x<45, a BCC phase is formed (Fig. 2.c.iii). Thus, $C_{\rm IM}^{\rm V~in~Ni}=45$ % and $C_{\rm IM}^{\rm Ni~in~V}=18$ %.

The same evaluation has been carried out for all the here considered element-impurity combinations to determine 110 $C_{\rm IM}$ values (Table 1, Fig. 3, Supplementary Table 1). $C_{\rm IM}$ values vary between 5 % and 100 %. Of note, 47 element-impurity combinations exhibit a $C_{\rm IM}$ of 100 %, which are ~40 % of the considered binary systems. $C_{\rm IM}=100$ %

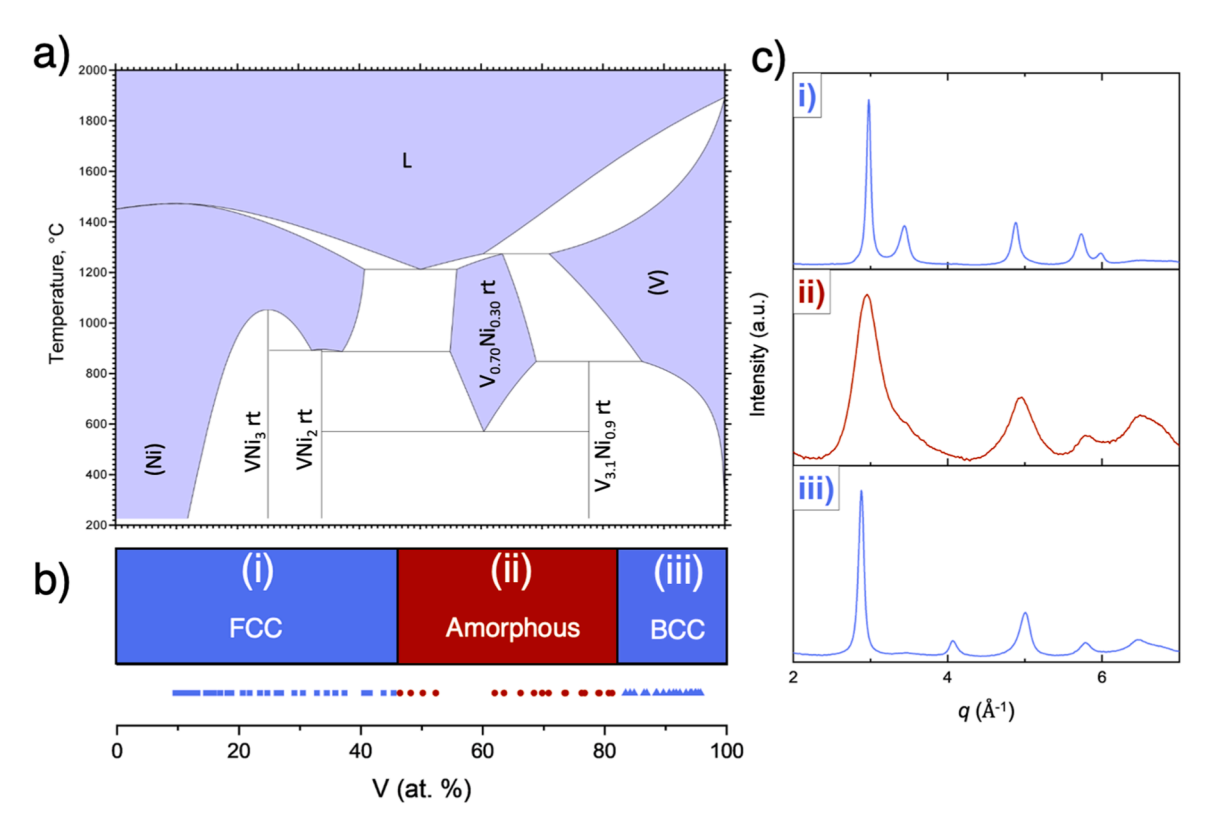


Fig. 2. $C_{\rm IM}$ for V in Ni and Ni in V impurity-base element combinations. a.) Ni-V phase diagram (from ASM database) b.) Summary of the evaluation of the sputtered data revealing composition range that forms FCC (blue squares), amorphous (red circles), and BCC (blue triangles). c.) Corresponding representative XRD spectra of the FCC phase (i), amorphous phase (ii) and BCC phase (iii). (color in print & online).

suggests a benign effect of the impurity on the base, though among this set of impurities-base element combinations, it is not possible to differentiate which are most benign, as this is indistinguishable at these cooling rate. Further, within one binary combination, the $C_{\rm IM}$ can also be very different for A in B and B in A; for example, in the Al-Ni binary, Ni is quite tolerant to Al impurities ($C_{\rm IM}^{\rm Al~in~Ni}=65$ %) while Al is very sensitive to Ni impurities ($C_{\rm IM}^{\rm Ni~in~Al}=12$ %).

4. Discussion

In the following, we will discuss why $C_{\rm IM}$ offers itself to indicate impurity tolerance, how $C_{\rm IM}$ differs from other parameters that may also be associated with impurity tolerance, and if and how one can estimate an impurity's effect on an alloy from the effect on its constituent elements.

4.1. Why does C_{IM} correlate with impurity tolerance?

 $C_{\rm IM}$ represents the effect of an impurity on a base element that causes a measurable and well-defined phase change. We argue that this value directly correlates with the tolerance of the base element, hence, inversely correlates with the impact of the impurity, by considering the "atomic dispersity", which describes similarities of alloying elements [46]. This concept has been used to compare the most common thermodynamic and kinetic rules for solidification and phase formation (Supplementary Discussion). Most notable are the Hume-Rothery rules (1926), which lay out requirements for the formation of solid solutions [51,52], whereas Inoue's rules (2000) specify requirements for bulk glass formation [53]. In the framing of atomic dispersity, solid solutions require elements of low dispersity, and enhancing metallic glass formation requires elements of high dispersity [46]. For similar arguments that justify Hume-Rothery and Inoue rules, one can argue that the $C_{\rm IM}$ impurity tolerance can be described by the dispersity of the impurity and

the element. For good glass formers, one can expect that only a small quantity of an impurity with high dispersity from the base element is sufficient to reduce the critical cooling rate for glass formation from $\sim \! 10^{14}$ K/s which is common amongst pure metal elements [31] to the 10^8 K/s when measuring $C_{\rm IM}$ during sputtering, hence resulting in a small $C_{\rm IM}$. This high dispersity mixture would also be less likely to form a solid solution, by the Hume-Rothery rules, and thus would lead to microstructural changes if fabricated in the bulk form. If, on the other hand, an impurity-element alloy is a poor glass former, the base element and impurity would have a low dispersity, and the gradual addition of the impurity to the base element would only slowly decrease the critical cooling rate, thus requiring a large amount of added impurity to form a glass. In that case, one would measure a large $C_{\rm IM.}$, and one would expect the elemental binary to easily form a solid solution, hence a less likely impact on the microstructure and a higher impurity tolerance.

It is important to address if there are other measures besides the here proposed $C_{\rm IM}$ that can also indicate impurity tolerance and, if so, how these other measures correlate with $C_{\rm IM}$. Based off the Hume-Rothery and Inoue rules, we can focus on properties important to phase formation in alloys. These are the crystal structure of the constituents, mixing enthalpies, electronegativity difference, valency matching, and atomic radius difference. When plotting $C_{\rm IM}$ values against these properties, very weak correlations and a large scatter are revealed (Fig. 4a-e). Clearly, no single parameter can replace $C_{\rm IM}$. This is not surprising, as also Hume-Rothery and Inoue rules are based on a multitude of requirements.

One could also argue that the solid solubility limit (SSL) in equilibrium phase diagrams could be considered as an indicator for impurity tolerance. SSL, considered here as the maximum solubility, varies from very small values < 0.1 at.% to complete solubility. However, we find only a very weak linear correlation of SSL with $C_{\rm IM}$ (R² = 0.21) and a large scatter (Fig. 4f). To understand this finding, it is important to state the differences between SSL and $C_{\rm IM}$. SSL reflects only equilibrium

 $c_{\rm IM}$ values for 110 out of the 1980 impurities-base element combinations.

	Impurity	ity																						
Base		Ag	Al	Au	Co	Cr	Cu	Fe	સુ	JH	Mg	Mn	Mo	Nb	Ni	Ьd	Pt	Si	Sn T	Ta Ti	Λ !	W	Y	Zr
	Ag	ı	100	ı	ı	ı	ı	ı	ı	ı	ı	100	ı	ı	ı	ı	ı							I
	A	100	ı	100	ı	13	100	6	ı	16	32	11	ı	1	12	ı	1	1	1	. 23	3 14		I	ı
	Αn	1	100	1	ı	100	ı	ı	ı	40	43	ı	ı	1	1	ı	1		1	1				
	ဝ	1	ı	1	ı	51	ı	ı	ı	ı	7	ı	ı	1	1	ı	1							
	Ċ	ı	26	100	38	1	ı	1	1	ı	31	ı	1	ı	100	ı	1	1	1	1	100	- 00	1	ı
	Cn	ı	100	1	ı	1	1	1	1	1	8	ı	100	1	100	1	1							
	Fe	ı	69	ı	ı	ı	ı	ı	ı	21	42	ı	ı	1	ı	100	1							
	Ge	ı	ı	ı	ı	ı	ı	ı	ı	ı	0	ı	ı	ı	1	ı	0							
	ΗĘ	ı	12	17	ı	ı	ı	2	ı	I	100	ı	ı	ı	ı	ı	ı							
	Mg	1	28	16	56	39	12	36	34	100	1	46	100	100	6	24	10							
	Mn	100	16	1	ı	ı	ı	ı	ı	ı	10	ı	ı	1	ı	1	1							
	Mo	1	1	1	ı	ı	100	1	1	1	100	1	ı	1	1	1	1			- 10				
	Nb	1	1	1	ı	ı	1	1	1	1	100	1	ı	1	1	1	1						_	
	Ä	ı	9	ı	ı	100	100	ı	ı	ı	6	ı	ı	ı	ı	1	1							
	Ьd	ı	ı	ı	ı	ı	ı	100	ı	ı	46	ı	ı	ı	ı	1	ı							
	Pt	ı	ı	ı	ı	ı	ı	ı	48	ı	9/	ı	ı	1	1	1	1							
	Si	ı	ı	ı	ı	ı	0	ı	ı	ı	ı	ı	ı	1	1	1	1							
	Sn	ı	ı	ı	ı	ı	ı	ı	ı	ı	100	ı	ı	1	1	1	1							
	Та	1	ı	1	ı	1	ı	1	ı	ı	100	2	ı	1	1	1	1							
	Ή	1	20	1	ı	ı	ı	1	ı	100	100	ı	100	1	1	1	1							
	>	ı	63	ı	ı	100	100	ı	ı	20	27	ı	ı	ı	19	1	ı	14						
	M	ı	ı	1	ı	ı	1	ı	ı	ı	45	ı	ı	100	1	ı	ı							
	Y	ı	ı	ı	ı	ı	ı	ı	ı	100	ı	ı	ı	1	1	1	ı	1	1					
	Zr	ı	ı	ı	ı	ı	8	ı	ı	100	ı	ı	19	ı	ı	1	ı							

conditions, whereas C_{IM} considers also non-equilibrium conditions. Further, SSL does not indicate a ubiquitous transition from the base crystal structure to a two-phase equilibrium with the impurity element's crystal phase, but rather a two-phase equilibrium with the closest following phase, which can include a wide range of intermetallic compounds. As these different phases cover a wide range of possibilities within binary combinations of elements, the transition from base crystal structure (which is always FCC, HCP, or BCC) to this secondary phase can be very different across binary alloys combinations. Hence, SSL is alloy specific and indicates the transition of these two phases under equilibrium conditions and does not allow a more general comparison. Incidentally, SSL and glass forming ability have been reported to not be correlated, and the lack of such correlation has been explained by similar arguments as used here for the absence of a correlation between $C_{\rm IM}$ and SSL [54]. By contrast, $C_{\rm IM}$ measures the transition in an alloy as a function of composition from the base crystal structure to the amorphous phase, a more consistent and, therefore, broadly comparable change.

Rather than manually parsing alloying indicators as in Fig. 4, tools based on CALPHAD (CALculation of PHAse Diagrams) can make predictions of how impurities affect phase stability based on curated thermodynamic and experimental parameters. These predictions can give estimates of stability ranges like SSL based on the equilibrium base structure and intermetallic phases, and this practical tool has enabled huge strides in metallurgical development. However, the general finding in the published literature does not support an indication of impurity tolerance by the SSL, as SSL does not correlate with properties changes due to impurities compositions below the SSL [55] nor does it indicate the rate of microstructure change above the SSL [56,57], which is also supported by our evaluation of impurity tolerance below. This may indicate that phase stability in equilibrium is insufficient to describe the complex characteristic of impurity tolerance, in particular when considering non-equilibrium conditions. In contrast to SSL, $C_{\rm IM}$, even though indirect, represents non-equilibrium thermodynamic and kinetic contributions on phase selection, microstructures, and properties, thus offering complimentary information to existing tools understandings.

 C_{IM} is proposed here to generally indicate the effect of an impurity on an alloy. However, for the same reason that determining impurity tolerance for all impurity-alloy combinations is generally an incommensurable task, it is also challenging to broadly validate C_{IM} as an indicator for impurity tolerance. In an attempt to show how to use C_{IM} , we consider the well-studied Ti-6Al-4 V alloy. Here, the Al-rich α phase and V-rich β phase determine the alloy's mechanical properties [58–61]. The effect of an impurity on Ti-6Al-4 V can be estimated by the effect on these phases which, as discussed in Fig. 5, can be estimated by the effect on the constitutive elements. For example, the low $C_{\mathrm{IM}}^{\mathrm{Si~in~V}}=14$ % would indicate a low tolerance of the V-rich β phase to Si. This has indeed be observed, as minor Si additions affect creep resistance due to rejection from the β phase [62]. Further, the low $\textit{C}_{IM}^{Mn~in~Al}=11$ % predicts a low tolerance of Al-rich α phase to Mn. Also this has been observed, Mn significantly impacts the a phase, leading to changes in hardness and corrosion resistance [63].

This case example somewhat validates the potential of $C_{\rm IM}$ to predict impact on phases and illustrates how to use this tool to evaluate other impurity-alloy effects at a high level. However, it should not be mistaken for a quantitative predictor of specific properties, as it lacks the necessary complexity to fully capture these. The offered value of this indicator, rather, is to anticipate that the microstructure may be impacted which, in turn, affects material properties. With the help of $C_{\rm IM}$, this possibility could be identified and further characterized through traditional methods if needed. Further, particularly when considering the already significant number of 110 out of the 1980 impurities-base metal combinations determined here, $C_{\rm IM}$ offers itself as a practical tool to design new alloys through computations where impurity tolerance can

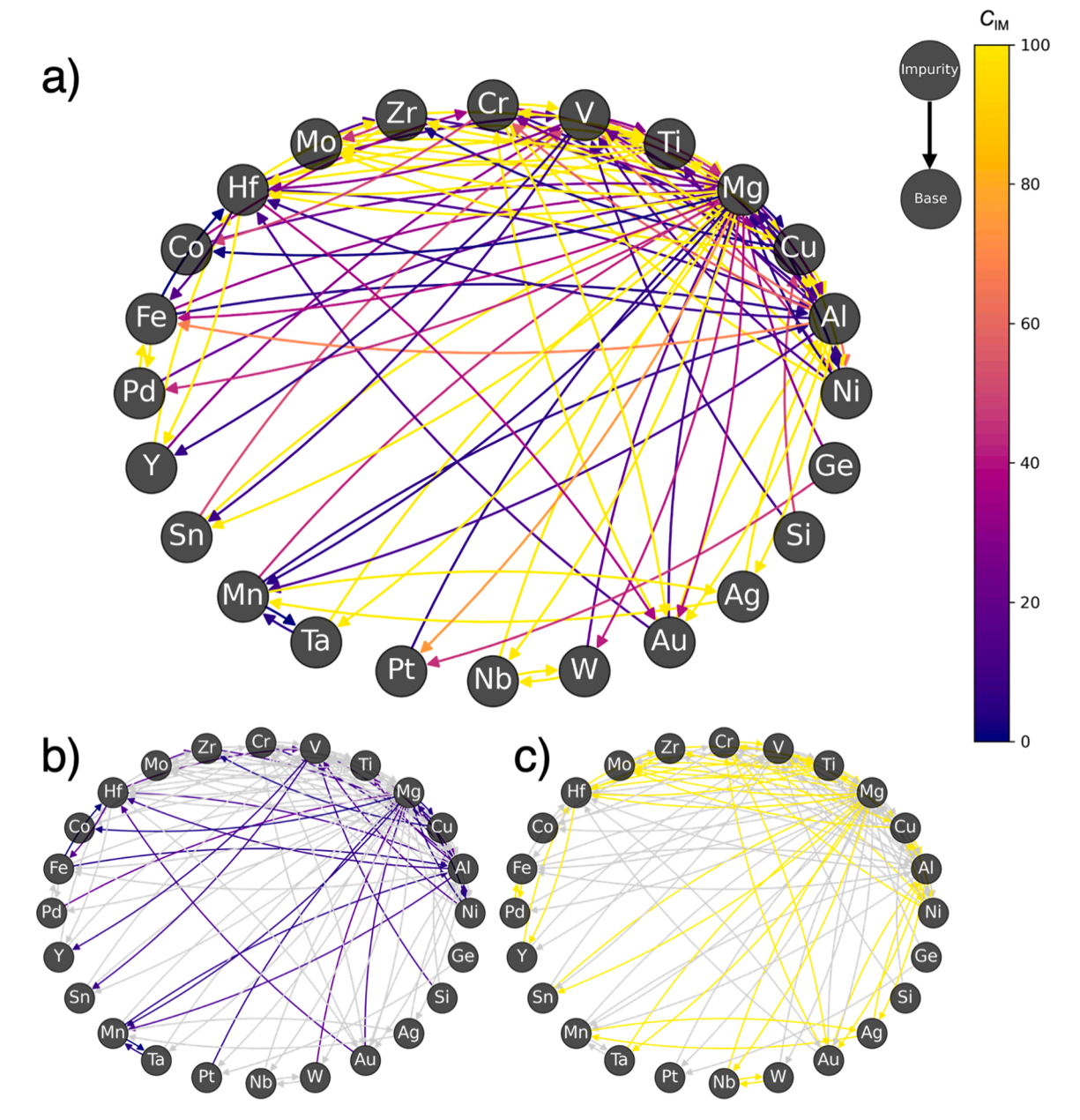


Fig. 3. Network visualization of measured C_{IM} values, exhibiting weighted (0 to 100, purple to yellow) directional (arrows pointing from impurity to base element) edges. Isolated are b) the most impactful (purple, $C_{\text{IM}} < 20$ %) and c) benign (yellow, $C_{\text{IM}} > 80$ %) impurity-base element combinations. (color in print & online).

be considered in the alloy design process (by avoiding alloy combinations with small $C_{\rm IM}$ values, see Fig. 6).

4.2. Impurity tolerance and microstructures

While the $C_{\rm IM}$ indicator cannot predict precise changes in chemistry, specific intermetallic phase formation, or grain boundary precipitates, it does generally indicate stability of the primary phase and should, in turn, qualitatively predict some changes in microstructure. As a first experimental attempt to validate $C_{\rm IM}$ as an indicator of bulk impurity tolerance, aluminum alloys were fabricated with impurities of a range of measured aluminum-impurity $C_{\rm IM}$ values, and the resulting microstructures were characterized. Aluminum was chosen as a base for its technological importance and known susceptibility to impurities [36, 64], and impurities were selected on the basis of exhibiting negligible equilibrium solid solubility in Al and a range of $C_{\rm IM}$ values. Further, the impurity levels (1 and 5 %) were intentionally selected as larger than

common industrial impurities (<0.5 %) for ease of observing a trend. Although comparing microstructures and extrapolating them to bulk properties can be difficult, they may offer a highly generalized view of impurity impacts on metals. We expect the rate of microstructure change with increasing impurity content should be large for the addition of an impurity with small $C_{\rm IM}$ (small impurity tolerance) and small for the addition of an impurity with large $C_{\rm IM}$ (high impurity tolerance). Stated differently, for the same absolute addition of an impurity to a base element, a larger change in microstructure should be generally present for a low $C_{\rm IM}$ pair than for a high $C_{\rm IM}$ pair. Here, we use only one of many possible methods to evaluate changes to the microstructure, and although it does not capture the full complexity of changes, it is useful as a first evaluation to measure grain size, which is generally associated with microstructure changes.

The results on the Al microstructures illustrate the capability of $C_{\rm IM}$: generally indicative of impurity impacts while imperfect as a highly precise predictive value. Low $C_{\rm IM}$ combinations are more sensitive to

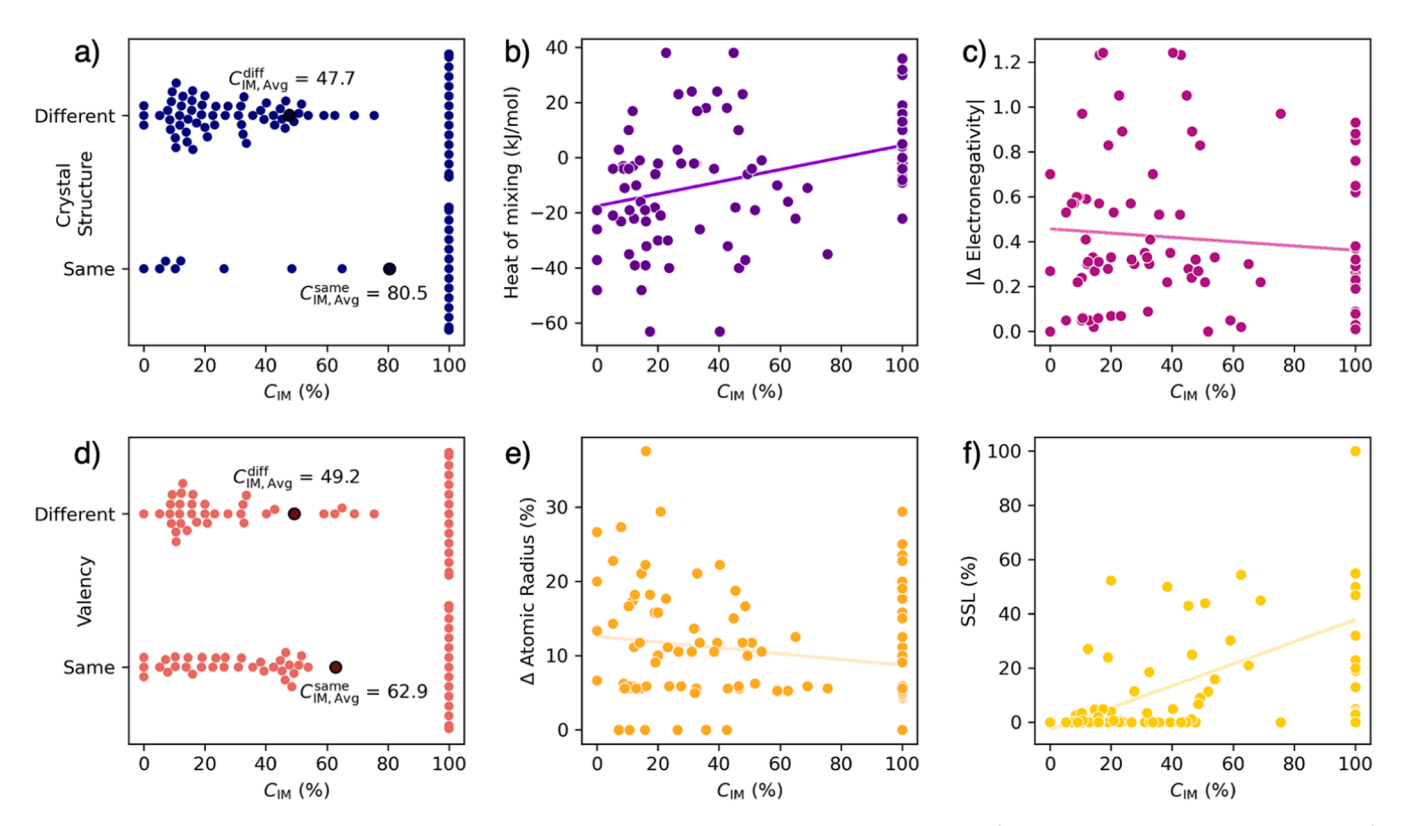


Fig. 4. Correlations between C_{IM} and various alloy characteristics such as a) crystal structure, b) heat of mixing ($R^2 = 0.17$), c) electronegativity difference ($R^2 = 0.014$), d) valency, e) atomic radius difference ($R^2 = 0.033$), and f) solid solubility limit ($R^2 = 0.21$). None of the considered alloy characteristics exhibit a significant correlation with C_{IM} . (color in print & online).

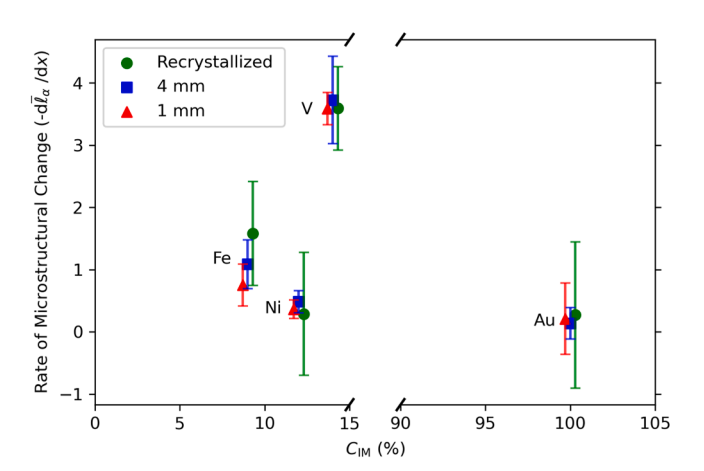


Fig. 5. The effect of impurities on the lengthscale change of Al microstructures, organized by $C_{\rm IM}$ values. The change in \bar{l}_a with added impurity from 1 to 5 % $(d\bar{l}_a/dx)$ is determined for the four impurities (Au, Ni, V, Fe) and the three processing conditions (as-cast in 1 mm and 4 mm copper molds and recrystallized). (color in print & online).

impurities, exhibiting microstructures with larger rates of change with added impurity (Al-V, Fig. 5), greater dependence on cooling conditions (Al-Fe, Fig. 5), or significant changes to precipitate geometry at higher impurity levels (Al-Ni, supplementary figure 1). In the evaluated high $C_{\rm IM}$ species (Al-Au), the effect of the impurity on the microstructure is comparatively stable across cooling conditions and has a minor rate of change with added impurity. Further the results reveal that SSL is not an adequate predictor of impurity tolerance reflecting in the microstructure, as all analyzed impurities exhibit essentially identical solid solubility in Al (< 0.1 %) but result in very different microstructural

changes. Obviously, this subset of microstructure data is only a minute fraction of all possible alloy-impurity microstructures, thereby showing a highly incomplete picture. As already discussed further above, a full correlative evaluation of $C_{\rm IM}$ and microstructural change, or any other bulk material property for that matter, would require the fabrication and characterization of a vast quantity of alloys [54], a daunting task even when considering high-throughput techniques [65–69]. Thus, a true validation of $C_{\rm IM}$ can only come with time, uptake, and evaluation by the material science community.

4.3. From elemental to alloy impurity tolerance

The majority of practical interests are in the effect of an impurity on an alloy rather than on a pure element. Experimentally determining the impurity tolerance of all possible impurities for all alloys is an unmanageable task when considering that there are $\sim 10^{12}$ quinary alloys [54].

The question then is: is it possible to estimate the effect of an impurity on an alloy from the effects of the impurity on the alloy's constituent elements? Generally, predicting alloy properties from constituent properties is highly unreliable. Alloys comprise typically of multiple phases, which can be solid solutions or intermetallic phases. Every phase can have a different composition, and typically they solidify sequentially in a difficult-to-predict sequence. Predicting the effect of an impurity on an alloy therefore becomes difficult. However, $C_{\rm IM}$ can be useful to make informed estimates on how an impurity affects each individual phase in the alloys' microstructure. For the sake of simplicity, we continue the discussion with a general binary alloy XY with impurity Z, where $C_{\rm IM}^{z~in~X}$ and $C_{\rm IM}^{z~in~Y}$ are known, and we discuss possibilities for concluding $C_{\rm IM}^{z~in~X}$ and $C_{\rm IM}^{z~in~Y}$ are known, and we discuss possibilities for concluding $C_{\rm IM}^{z~in~X}$ (Fig. 6).

Two classes of phases are the building blocks of all crystalline microstructures: solid solutions and intermetallics. Solid solutions exhibit the same crystal structure as the pure base element. Hence, particularly for small amounts of Y, $C_{IM}^{Z\ in\ XY}\cong C_{IM}^{Z\ in\ X}$. If Y is fully soluble in X (low

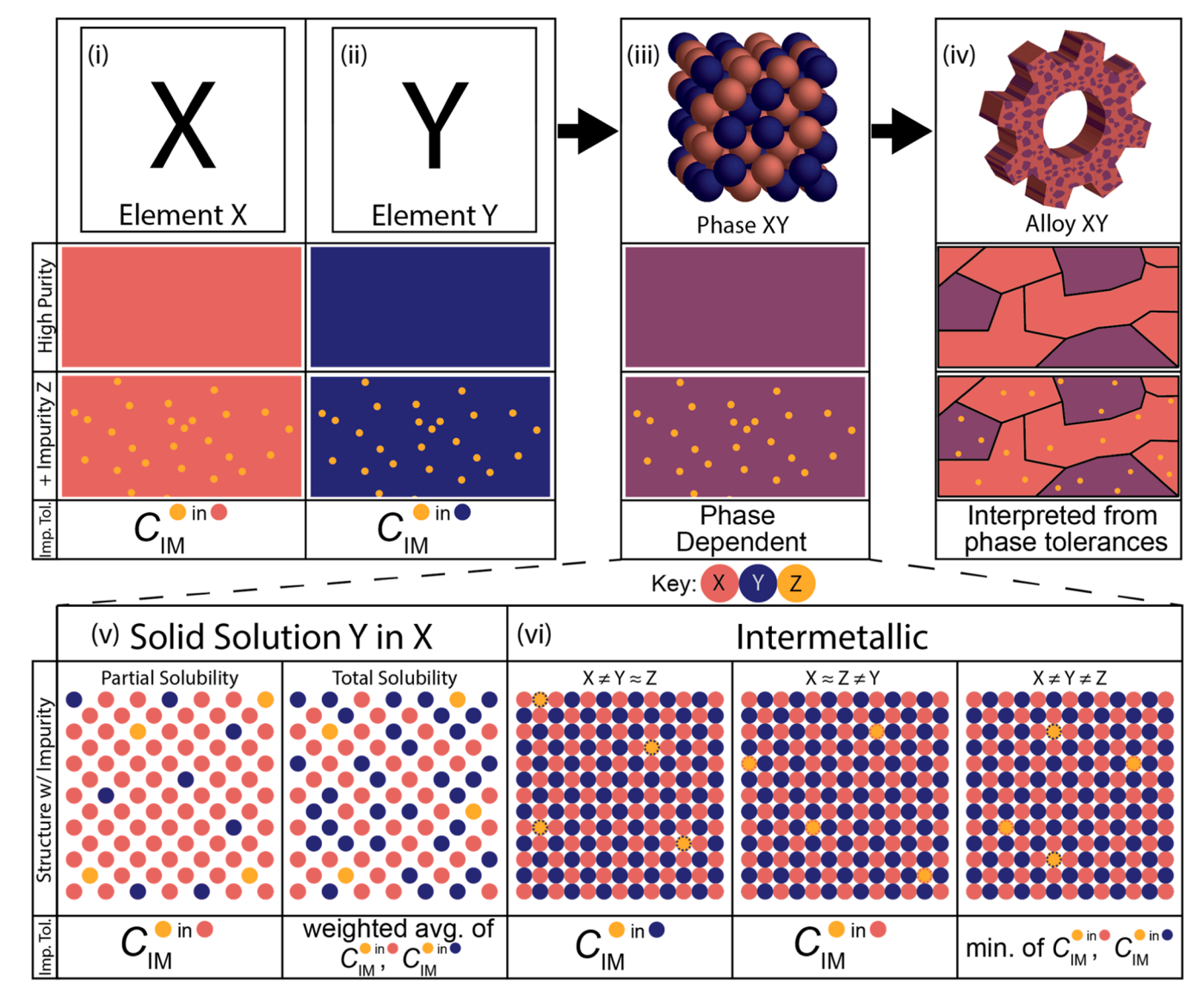


Fig. 6. Interpreting impurity tolerance of alloys from impurity tolerance of elements. For the generic case of alloy XY with impurity Z, the known C_{IM} impurity tolerances of elements X (i) and Y (ii) to Z can be used to approximate the impurity tolerance of any XY phase (iii) to Z. In turn, the effect of Z on the XY alloy (iv) can be interpreted via the effects on the constituent phases. The impurity tolerance of phases can be approximated for both solid solutions (v) and intermetallics (vi) using the composition of the phase and dispersity of the elements. (color in print & online).

dispersity) for a given composition, one can conclude $C_{IM}^{Z\ in\ XY}\cong C_{IM}^{Z\ in\ X}\cong C_{IM}^{Z\ in\ Y}$ (Fig 6.v). In the case of an intermetallic phase X_mY_n (high dispersity), we must consider the effect of Z on each of the sublattices of the phase X_mY_n by considering their atomic dispersity. Here, two practical scenarios exist: Z is similar to one sublattice and highly disperse from the other (i.e., $Z\cong X, Z\neq Y$) or Z is highly disperse from both sublattices (i.e., $Z\neq X, Z\neq Y$). The case of Z being very similar to both sublattices typically does not exist, as otherwise no intermetallic would form but instead solid solutions. In the case of $Z\cong X$ and $Z\neq Y$, the impurity Z prefers to incorporate into the X sublattice and avoid the Y sublattice, forming a $(XZ)_mY_n$ intermetallic structure. Here, $C_{IM}^{Z\ in\ X_mY_n}\cong C_{IM}^{Z\ in\ X}$ (Fig 5.vi). For the other case of $Z\neq X$ and $Z\neq Y$, $C_{IM}^{Z\ in\ X_mY_n}$ will be set by the lesser of $C_{IM}^{Z\ in\ Z}$ and $C_{IM}^{Z\ in\ Y}$. Assuming $C_{IM}^{Z\ in\ X} < C_{IM}^{Z\ in\ Y}$, we can conclude $C_{IM}^{Z\ in\ X_mY_n} < C_{IM}^{Z\ in\ X}$ (Fig 6.vi). However, it is generally not possible to conclude by how much $C_{IM}^{Z\ in\ X_mY_n}$ is smaller than $C_{IM}^{Z\ in\ X}$. This is most extreme for line phases which require very specific compositions, and a large fraction of intermetallics are line phases.

The above discussion suggests some conclusions about the impurity

tolerance of metallic phases from the known impurity tolerances of the constituent elements. Direct conclusions about impurity tolerances of alloys from impurity tolerances of phases/elements are generally not possible, as more information about the alloy would be needed, including the phase chemistry and solidification order. Further, this general framework does not account for the complexities of the most general case of a multi-component, multi-phase alloy with multiple impurities. However, $C_{\rm IM}$ impurity tolerance coupled with a metallurgical understanding of the role each phase plays in the properties would allow one to begin to interpret the effects of impurities on the alloy as a whole.

5. Conclusions

We propose a high-level indicator for the impurity tolerance of alloys. For this, combinatorial synthesis and high-throughput characterization are used to determine a representative fraction of all practical binary combinations of impurity-(metal) element combinations. This practical and versatile indicator, $C_{\rm IM}$, which is quantified as the

maximum content an element A can tolerate of element B before it vitrifies into an amorphous phase under as-sputtered conditions, generally represents the magnitude of effects on microstructure of B on A. C_{IM} reflects a multitude of thermodynamic and kinetic contributions which we argue are also the contributions controlling phase selection and microstructure of alloys. Connections are drawn between the effect of an impurity on elements with the effect of this impurity on an alloy phase comprised of these elements, and we offer strategies on how to connect this knowledge with the effect of this impurity on the alloy. These qualitative predications can aid in inferring potentially impacted properties, provided there is an existing understanding of the microstructure-property relationships for the alloy of interest. While $C_{\rm IM}$ may offer low predictability for a specific situation, it can provide a high-level knowledge about general trends in impurity tolerance, which we expect to be important in sustainable use of current alloys, response to changing supply chains, and design of new alloys. Especially with the ever-increasing complexity of modern alloys, many of which involve critical metals, a more practical understanding of impurities is required, otherwise these alloys' main alloying elements will likely be relegated to a single use before being non-functionally recycled or discarded altogether.

Data availability

The raw data generated during this study are available from the corresponding author on reasonable request.

Authors contributions

E.T.L., S.S., and J.S. designed this study. S.A.K. designed the sputtering strategy and high throughput analysis. S.H. and S.A.K. performed the EDS experiments. S.H., S.A.K., N.J., G.L, and A.M. performed the XRD experiments. E.T.L., S.H., S.S., and J.S. analyzed the EDS and XRD results. E.T.L. and W.C. performed microstructure experiments. E.T.L., S. A.K, and J.S. wrote the initial draft of the paper. S.H., S.S., and B.K.R. contributed to revisions and editing of the paper. All authors contributed to the discussion and finishing of the final paper.

Declaration of competing interest

The authors declare that they have no known competing financial interests or personal relationships that could have appeared to influence the work reported in this paper.

Acknowledgements

This work was supported by NSF DMR through award #2104316. X-ray diffraction data were collected at the Stanford Synchrotron Radiation Lightsource, SLAC National Accelerator Laboratory, which is supported by the U.S. Department of Energy, Office of Science, Office of Basic Energy Sciences under Contract No. DE-AC02–76SF00515. This material is based upon work supported by the National Science Foundation Graduate Research Fellowship under Grant No. 2139841.

Supplementary materials

Supplementary material associated with this article can be found, in the online version, at doi:10.1016/j.mtla.2024.102037.

References

- D. Raabe, C.C. Tasan, E.A. Olivetti, Strategies for improving the sustainability of structural metals, Nature 575 (7781) (2019) 64–74.
- [2] M.A. Reuter, A. van Schaik, J. Gutzmer, N. Bartie, A. Abadías-Llamas, Challenges of the circular economy: a material, metallurgical, and product design perspective, Annu. Rev. Mater. Res. 49 (1) (2019) 253–274.

[3] E.V. Verhoef, G.P.J. Dijkema, M.A. Reuter, Process knowledge, system dynamics, and metal ecology, J. Ind. Ecol. 8 (1–2) (2004) 23–43.

- [4] G. Gaustad, E. Olivetti, R. Kirchain, Improving aluminum recycling: a survey of sorting and impurity removal technologies, Resour. Conser. Recycl. 58 (2012) 79–87
- [5] G.W. Meetham, Trace elements in superalloys—an overview, Metals Technol. 11 (1) (1984) 414–418.
- [6] X. Lu, K. Matsubae, K. Nakajima, S. Nakamura, T. Nagasaka, Thermodynamic considerations of contamination by alloying elements of Remelted End-of-Life Nickel- and Cobalt-Based Superalloys, Metallurg. Mater. Trans. B 47 (3) (2016) 1785–1795
- [7] E.C. Bain, H.W. Paxton, Alloying elements in steel, 1966, 291 P AMERICAN SOCIETY FOR METALS, Metals Park, OHIO (1966).
- [8] N. Imai, N. Komatsubara, K. Kunishige, Effect of Cu, Sn and Ni on hot workability of hot-rolled mild steel, ISIJ Int. 37 (3) (1997) 217–223.
- [9] C. Lee, S.-J. Kim, T.-H. Lee, C.-S. Oh, Effects of tramp elements on formability of Low-carbon TRIP-aided multiphase cold-rolled steel sheets, Isij Int. - ISIJ INT 44 (2004) 737–743.
- [10] I. Daigo, L. Fujimura, H. Hayashi, E. Yamasue, S. Ohta, T.D. Huy, Y. Goto, Quantifying the total amounts of tramp elements associated with carbon steel production in Japan, ISIJ Int. 57 (2) (2017) 388–393.
- [11] J.R. Davis, Aluminum and aluminum alloys, ASM Int. (1993).
- [12] E.L. Rooy, Introduction to aluminum and aluminum alloys, in: Metals Handbook, 2, ASM International, 1990, pp. 3–14. Tenth Edition.
- [13] T. Kobayashi, Strength and fracture of aluminum alloys, Mater. Sci. Eng.: A 280 (1) (2000) 8–16.
- [14] H. Berns, W. Theisen, Ferrous Materials: Steel and Cast Iron, Springer Science & Business Media, 2008.
- [15] M.A. Tayeb, S. Spooner, S. Sridhar, Phosphorus: the noose of sustainability and renewability in steelmaking, JOM 66 (9) (2014) 1565–1571.
- [16] H. Tervo, A. Kaijalainen, T. Pikkarainen, S. Mehtonen, D. Porter, Effect of impurity level and inclusions on the ductility and toughness of an ultra-high-strength steel, Mater. Sci. Eng.: A 697 (2017) 184–193.
- [17] J.C. Herman, V. Leroy, Influence of residual elements on steel processing and mechanical properties, Iron Steelmaker 23 (1996) 35–43.
- [18] J. Zhang, H. Chen, D. Fan, J. Huang, X. Yu, W. Feng, K. Xu, Effects of phosphorus impurity on the microstructure and impact toughness of weld joint for the 12Cr2Mo1R heat resistant steel, J. Manuf. Process. 38 (2019) 453–461.
- [19] A.A. Hermas, M.S. Morad, K. Ogura, A correlation between phosphorous impurity in stainless steel and a second anodic current maximum in H2SO4, Corros. Sci. 41 (12) (1999) 2251–2266.
- [20] N. Ånmark, A. Karasev, P.G. Jönsson, The effect of different non-metallic inclusions on the machinability of steels, Materials (Basel) 8 (2) (2015) 751–783.
- [21] L. Xie, T. Liu, A. He, Q. Li, Z. Gao, A. Wang, C. Chang, X. Wang, C.T. Liu, High Bs Fe-based nanocrystalline alloy with high impurity tolerance, J. Mater. Sci. 53 (2) (2018) 1437–1446.
- [22] K.J. Harrelson, S.H. Rou, R.C. Wilcox, Impurity element effects on the toughness of 9Cr-1Mo steel, J. Nucl. Mater. 141-143 (1986) 508–512.
- [23] W.H. Wang, Roles of minor additions in formation and properties of bulk metallic glasses, Prog. Mater Sci. 52 (4) (2007) 540–596.
- [24] W. Chen, H.F. Zhou, Z. Liu, J. Ketkaew, N. Li, J. Yurko, N. Hutchinson, H.J. Gao, J. Schroers, Processing effects on fracture toughness of metallic glasses, Scripta Mater. 130 (2017) 152–156.
- [25] K. Nakajima, O. Takeda, T. Miki, K. Matsubae, S. Nakamura, T. Nagasaka, Thermodynamic analysis of contamination by alloying elements in aluminum recycling, Environ. Sci. Technol. 44 (14) (2010) 5594–5600.
- [26] M. Liu, G.-L. Song, Impurity control and corrosion resistance of magnesium–aluminum alloy, Corros. Sci. 77 (2013) 143–150.
- [27] B. Cantor, Impurity effects on heterogeneous nucleation, Mater. Sci. Eng.: A 226 (1997) 151–156.
- [28] M. Liu, P.J. Uggowitzer, A.V. Nagasekhar, P. Schmutz, M. Easton, G.-L. Song, A. Atrens, Calculated phase diagrams and the corrosion of die-cast Mg–Al alloys, Corros. Sci. 51 (3) (2009) 602–619.
- [29] J. Duan, D. Farrugia, C. Davis, Z. Li, Effect of impurities on the microstructure and mechanical properties of a low carbon steel, Ironmak. Steelmak. 49 (2) (2022) 140–146.
- [30] E.S. Park, H.J. Chang, J.S. Kyeong, D.H. Kim, Role of minor addition of metallic alloying elements in formation and properties of Cu-Ti-rich bulk metallic glasses, J. Mater. Res. 23 (7) (2008) 1995–2002.
- [31] L. Zhong, J.W. Wang, H.W. Sheng, Z. Zhang, S.X. Mao, Formation of monatomic metallic glasses through ultrafast liquid quenching, Nature 512 (7513) (2014), 177...
- [32] A.V. Pozdnyakov, R.Y. Barkov, Effect of impurities on the phase composition and properties of a New Alloy of the Al-Y-Er-Zr-Sc system, Metallurgist 63 (1) (2019) 79–86.
- [33] J.H. Li, B. Oberdorfer, S. Wurster, P. Schumacher, Impurity effects on the nucleation and growth of primary Al3(Sc,Zr) phase in Al alloys, J. Mater. Sci. 49 (17) (2014) 5961–5977.
- [34] R. Yamamoto, M. Doyama, O. Takai, The effect of impurities on diffusion in metals, Phys. Lett. A 44 (2) (1973) 105–106.
- [35] Y. Waseda, Minora Isshiki, Purification Process and Characterization of Ultra High Purity Metals, Application of Basis Science to Metallurgical Processing, Springer, New York, 2002.
- [36] D. Raabe, D. Ponge, P.J. Uggowitzer, M. Roscher, M. Paolantonio, C. Liu, H. Antrekowitsch, E. Kozeschnik, D. Seidmann, B. Gault, F. De Geuser, A. Deschamps, C. Hutchinson, C. Liu, Z. Li, P. Prangnell, J. Robson, P. Shanthraj,

- S. Vakili, C. Sinclair, L. Bourgeois, S. Pogatscher, Making sustainable aluminum by recycling scrap: the science of "dirty" alloys, Prog. Mater. Sci. 128 (2022) 100947.
- [37] M.R. Barnett, M. Senadeera, D. Fabijanic, K.F. Shamlaye, J. Joseph, S.R. Kada, S. Rana, S. Gupta, S. Venkatesh, A scrap-tolerant alloying concept based on high entropy alloys, Acta Mater. 200 (2020) 735–744.
- [38] L. Montanelli, E.R. Homer, E. Olivetti, Factors to consider when designing Aluminium alloys for increased scrap usage, in: A. Lazou, K. Daehn, C. Fleuriault, M. Gökelma, E. Olivetti, C. Meskers (Eds.) REWAS 2022: Developing Tomorrow's Technical Cycles (Volume I), Springer International Publishing, Cham, 2022, pp. 465–473.
- [39] J.L. Cann, A. De Luca, D.C. Dunand, D. Dye, D.B. Miracle, H.S. Oh, E.A. Olivetti, T. M. Pollock, W.J. Poole, R. Yang, C.C. Tasan, Sustainability through alloy design: challenges and opportunities, Prog. Mater. Sci. 117 (2021).
- [40] M.J. Eckelman, L. Ciacci, G. Kavlak, P. Nuss, B.K. Reck, T.E. Graedel, Life cycle carbon benefits of aerospace alloy recycling, J. Clean. Prod. 80 (2014) 38–45.
- [41] UNEP, Environmental risks and challenges of anthropogenic metals flows and cycles, a report of the working group on the Global Metal flows to the international resource panel, in: E.S. van der Voet, R.; Eckelman, M.; Mudd, G.; Norgate, T.; Hischier, R. Paris (Ed.), UNEP DTIE, Sustainable Consumption and Production Branch (2013)
- [42] T.E. Graedel, E.M. Harper, N.T. Nassar, P. Nuss, B.K. Reck, Criticality of metals and metalloids, Proc. Natl. Acad. Sci. U. S. A. 112 (14) (2015) 4257–4262.
- [43] P. Nuss, E.M. Harper, N.T. Nassar, B.K. Reck, T.E. Graedel, Criticality of iron and its principal alloying elements, Environ. Sci. Technol. 48 (7) (2014) 4171–4177.
- [44] T.E. Graedel, B.K. Reck, A. Miatto, Alloy information helps prioritize material criticality lists, Nat. Commun. 13 (1) (2022) 150.
- [45] P.T. Anastas, J.B. Zimmerman, Design through the 12 principles of green engineering, Environ. Sci. Technol. 37 (5) (2003) 94A–101A.
- [46] S.A. Kube, J. Schroers, Metastability in high entropy alloys, Scripta Mater. 186 (2020) 392–400.
- [47] N.J. Liu, T.X. Ma, C.Q. Liao, G.N. Liu, R.M.O. Mota, J.B. Liu, S. Sohn, S. Kube, S. F. Zhao, J.P. Singer, J. Schroers, Combinatorial measurement of critical cooling rates in aluminum-base metallic glass forming alloys, Sci. Rep.-Uk 11 (1) (2021).
- [48] R.M.O. Mota, T.E. Graedel, E. Pekarskaya, J. Schroers, Criticality in bulk metallic glass constituent elements, JOM 69 (11) (2017) 2156–2163.
- [49] S. Curtarolo, W. Setyawan, S. Wang, J. Xue, K. Yang, R.H. Taylor, L.J. Nelson, G.L. W. Hart, S. Sanvito, M. Buongiorno-Nardelli, N. Mingo, O. Levy, AFLOWLIB.ORG: a distributed materials properties repository from high-throughput ab initio calculations, Comput. Mater. Sci. 58 (2012) 227–235.
- [50] S. Ding, Y. Liu, Y. Li, Z. Liu, S. Sohn, F. Walker, J. Schroers, Combinatorial development of Metallic Glasses, Nat. Mater. 13 (2014) 494.
- [51] W. Hume-Rothery, Researches on the Nature, Properties, and Conditions of Formation of Intermetallic Compounds, with Special Reference to Certain Compounds of Tin, University of London, 1926.
- [52] W. Hume-Rothery, The structure of metals and alloys, Nature 138 (3479) (1936)
- [53] A. Inoue, Stabilization of metallic supercooled liquid and bulk amorphous alloys, Acta Mater 48 (1) (2000) 279–306.

- [54] Y.L. Li, S.F. Zhao, Y.H. Liu, P. Gong, J. Schroers, How Many Bulk Metallic Glasses Are There? Acs Comb Sci 19 (11) (2017) 687–693.
- [55] H.A. Roth, C.L. Davis, R.C. Thomson, Modeling solid solution strengthening in nickel alloys, Metall. Mater. Trans. A 28 (6) (1997) 1329–1335.
- [56] S. Zhu, J.-Y. Yao, L. Sweet, M. Easton, J. Taylor, P. Robinson, N. Parson, Influences of nickel and vanadium impurities on microstructure of aluminum alloys, JOM 65 (5) (2013) 584–592.
- [57] J. Rakhmonov, G. Timelli, F. Bonollo, The effect of transition elements on high-temperature mechanical properties of Al–Si foundry Alloys–a review, Adv. Eng. Mater. 18 (7) (2016) 1096–1105.
- [58] G. Lütjering, Influence of processing on microstructure and mechanical properties of (α+β) titanium alloys, Mater. Sci. Eng.: A 243 (1) (1998) 32-45.
- [59] S. Sun, D. Zhang, S. Palanisamy, Q. Liu, M.S. Dargusch, Mechanical properties and deformation mechanisms of martensitic Ti6Al4V alloy processed by laser powder bed fusion and water quenching, Mater. Sci. Eng. A 839 (2022).
- [60] B. Ahn, Microstructural tailoring and enhancement in compressive properties of additive manufactured ti-6al-4v alloy through heat treatment, Materials (Basel) 14 (19) (2021).
- [61] I. Sen, S. Tamirisakandala, D.B. Miracle, U. Ramamurty, Microstructural effects on the mechanical behavior of B-modified Ti-6Al-4V alloys, Acta Mater. 55 (15) (2007) 4983–4993.
- [62] Y. Li, Y. Chen, J.-R. Liu, Q.-M. Hu, R. Yang, Cooperative effect of silicon and other alloying elements on creep resistance of titanium alloys: insight from firstprinciples calculations, Sci. Rep. 6 (1) (2016) 30611.
- [63] J.-W. Kim, M.-J. Hwang, M.-K. Han, Y.-G. Kim, H.-J. Song, Y.-J. Park, Effect of manganese on the microstructure, mechanical properties and corrosion behavior of titanium alloys, Mater. Chem. Phys. 180 (2016) 341–348.
- [64] A. Lennon, M. Lunardi, B. Hallam, P.R. Dias, The aluminium demand risk of terawatt photovoltaics for net zero emissions by 2050, Nature Sustain. 5 (4) (2022) 357–363.
- [65] J. Cui, Y.S. Chu, O.O. Famodu, Y. Furuya, J. Hattrick-Simpers, R.D. James, A. Ludwig, S. Thienhaus, M. Wuttig, Z.Y. Zhang, I. Takeuchi, Combinatorial search of thermoelastic shape-memory alloys with extremely small hysteresis width, Nat. Mater. 5 (4) (2006) 286–290.
- [66] S.Y. Ding, Y.H. Liu, Y.L. Li, Z. Liu, S. Sohn, F.J. Walker, J. Schroers, Combinatorial development of bulk metallic glasses, Nat. Mater. 13 (5) (2014) 494–500.
- [67] Y.G. Yao, Z.N. Huang, T.Y. Li, H. Wang, Y.F. Liu, H.S. Stein, Y.M. Mao, J.L. Gao, M. L. Jiao, Q. Dong, J.Q. Dai, P.F. Xie, H. Xie, S.D. Lacey, I. Takeuchi, J.M. Gregoire, R. Z. Jiang, C. Wang, A.D. Taylor, R. Shahbazian-Yassar, L.B. Hu, High-throughput, combinatorial synthesis of multimetallic nanoclusters, P. Natl. Acad. Sci. U.S.A. 117 (12) (2020) 6316–6322.
- [68] M.X. Li, Y.T. Sun, C. Wang, L.W. Hu, S. Sohn, J. Schroers, W.H. Wang, Y.H. Liu, Data-driven discovery of a universal indicator for metallic glass forming ability, Nat. Mater. (2021).
- [69] R.K. Vasudevan, K. Choudhary, A. Mehta, R. Smith, G. Kusne, F. Tavazza, L. Vlcek, M. Ziatdinov, S.V. Kalinin, J. Hattrick-Simpers, Materials science in the artificial intelligence age: high-throughput library generation, machine learning, and a pathway from correlations to the underpinning physics, Mrs. Commun. 9 (3) (2019) 821–838.